Current Research in Structural Biology 2 (2020) 25–34

Contents lists available at ScienceDirect

Current Research in Structural Biology

journal homepage: www.journals.elsevier.com/current-research-in-structural-biology

Structural basis of elongation factor 2 switching

Michael K. Fenwick, Steven E. Ealick *

Department of Chemistry and Chemical Biology, Cornell University, Ithaca, NY, 14853, USA

ARTICLE INFO

Keywords:
Translation
Elongation factor
Translocase
Translocation
Ribosome
GTPase
Switch

ABSTRACT

Archaebacterial and eukaryotic elongation factor 2 (EF-2) and bacterial elongation factor G (EF-G) are five domain GTPases that catalyze the ribosomal translocation of tRNA and mRNA. In the classical mechanism of activation, GTPases are switched on through GDP/GTP exchange, which is accompanied by the ordering of two flexible segments called switch I and II. However, crystal structures of EF-2 and EF-G have thus far not revealed the conformations required by the classical mechanism. Here, we describe crystal structures of *Methanoperedens nitroreducens* EF-2 (*Mn*EF-2) and *Mn*EF-2-H595N bound to GMPPCP (GppCp) and magnesium displaying previously unreported compact conformations. Domain III forms interfaces with the other four domains and the overall conformations resemble that of SNU114, the eukaryotic spliceosomal GTPase. The gamma phosphate of GMPPCP is detected through interactions with switch I and a P-loop structural element. Switch II is highly ordered whereas switch I shows a variable degree of ordering. The ordered state results in a tight interdomain arrangement of domains I-III and the formation of a portion of a predicted monovalent cation site involving the P-loop and switch I. The side chain of an essential histidine residue in switch II is placed in the inactive conformation observed for the "on" state of elongation factor EF-Tu. The compact conformations of *Mn*EF-2 and *Mn*EF-2-H595N suggest an "on" ribosome-free conformational state.

1. Introduction

Archaebacterial and eukaryotic elongation factor 2 (EF-2) and bacterial elongation factor G (EF-G) catalyze the translocation of tRNA and mRNA from the aminoacyl site to the peptidyl site of the ribosome (Frank and Agrawal, 2000; Kaziro, 1978; Korostelev et al., 2008; Wintermeyer et al., 2001). Structurally, EF-2 and EF-G contain an amino terminal G domain (domain I), followed by a twisted β-barrel/β-sandwich domain (domain II) and three two-layer α-β sandwich domains (domains III-V), with that of domain IV displaying a unique topology (Aevarsson et al., 1994; Czworkowski et al., 1994; Jorgensen et al., 2003). Like other GTPases, the G domain of EF-2/EF-G contains a P-loop and two conformationally variable segments called switch I and switch II.

According to the classical mechanism of activation, GTPases are switched on by binding GTP and magnesium, which orders switch I and II to form a spring-loaded-like conformation (Vetter and Wittinghofer, 2001). Consistently, crystal structures of ribosome-bound EF-G in the GDP and GTP analog bound states show a disorder-to-order transition in switch I and a conformational change in switch II that are associated with an ordered arrangement of domains I-III that docks between the two ribosomal subunits (Gao et al., 2009; Pulk and Cate, 2013; Tourigny et al., 2013; Zhou et al., 2013); in the GDP bound state, switch I is disordered and domains III-V are dynamic (Fig. 1A) (Lin et al., 2015; Mace et al., 2018). However, crystal structures of ribosome-free EF-2, EF-G, and various active mutants bound to GDP or a GTP analog reported thus far show similar partially extended conformations that lack an ordered switch I (Fig. 1B), suggesting either that cocrystallization with particular GTP analogs makes difficult the capture of the "on" state or that the ribosome-free forms of these enzymes operate according to non-classical mechanisms (Aevarsson et al., 1994; Czworkowski et al., 1994; Jorgensen et al., 2003; al-Karadaghi et al., 1996; Hansson et al., 2005a; Koripella et al., 2012; Laurberg et al., 2000; Tanzawa et al., 2018).

Two notable explanations have been offered for why the ribosome-free structures of EF-2 and EF-G are inconsistent with the GTP on/off switch paradigm. The first is based on crystal structures of the fusidic acid resistant *Thermus thermophilus* EF-G-T84A mutant bound to GDP, GMPPNP (GppNp), or GMPPCP (PDB entries 2BM0, 2BV3, and 2J7K), which show similar extended conformations with a disordered switch I (Hansson et al., 2005a, 2005b). Hauryliuk et al. suggested a mechanism of conditional switching in which interaction with the ribosome leads to the conformational changes required for activation (Hauryliuk et al., 2008). The second explanation is based on crystal structures of a

* Corresponding author.
E-mail address: see3@cornell.edu (S.E. Ealick).

https://doi.org/10.1016/j.crstbi.2020.02.001
Received 13 September 2019; Received in revised form 7 February 2020; Accepted 14 February 2020

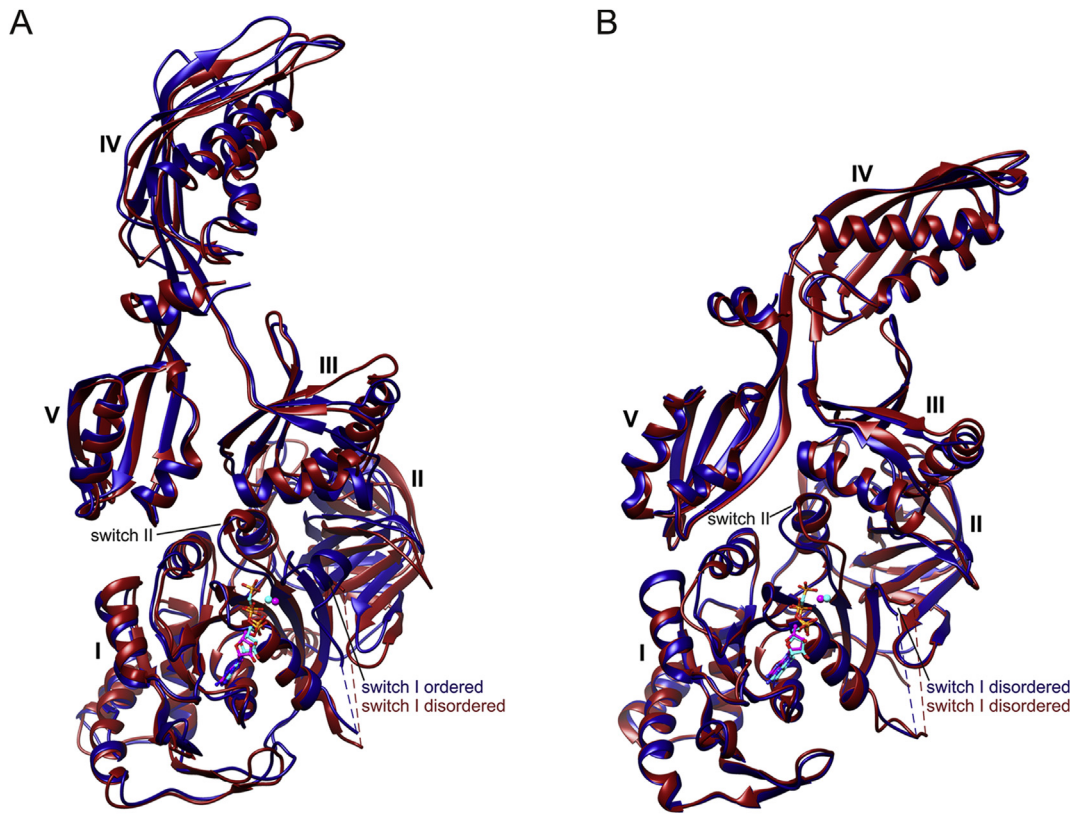

Fig. 1. Ribosome-bound and ribosome-free crystal structures of EF-G. (A) Structural superimposition of ribosome-bound *Escherichia coli* EF-G-GMPPCP-Mg^{2+} (PDB entry 4V9O; navy blue ribbons and cyan balls and sticks) (Pulk and Cate, 2013) and *Thermus thermophilus* EF-G-GDP-Mg^{2+} (PDB entry 4WQY; dark red ribbons and magenta balls and sticks) (Lin et al., 2015). (B) Structural superimposition of fusidic acid resistant ribosome-free *Tt*EF-G-T84A-GMPPCP-Mg^{2+} (PDB entry 2J7K; navy blue ribbons and cyan balls and sticks) (Hansson et al., 2005a) and *Tt*EF-G-T84A-GDP-Mg^{2+} (PDB entry 2BM0; dark red ribbons and magenta balls and sticks) (Hansson et al., 2005b). The T84A mutant is active (Martemyanov et al., 2001) and the overall conformations are similar to those of wild-type *Tt*EF-G (PDB entry 1ELO; not shown) (Aevarsson et al., 1994) and the active mutant *Tt*EF-G-H573A (PDB entry 1FNM; not shown) (Laurberg et al., 2000).

fragment of eukaryotic initiation factor 5B (eIF5B) bound to GTP or GTPγS (PDB entries 4TMW, 4TMV, and 4TMZ), which contain a monovalent cation coordinated by the α and γ-phosphate groups of the nucleotide, the oxygen atom bridging the β and γ-phosphate groups, and P-loop aspartate and switch I glycine residues that are conserved in other translational GTPases (Kuhle and Ficner, 2014). The monovalent cation binding site is distinct from the magnesium binding site, which involves different oxygen atoms of the β and γ-phosphate groups. Kuhle and Ficner suggested that the monovalent cation acts as a catalytic and structural cofactor and that disruption of the cation binding motif by insertion of an imido or methylene group between Pβ and Pγ in GMPPNP and GMPPCP, respectively, could account for the lack of an "on" state in currently available structures with these analogs bound (Kuhle and Ficner, 2014); similar effects have been noted for members of the cation-dependent GTPases (Ash et al., 2011; Chappie et al., 2011).

In this study, we describe crystal structures of *Methanoperedens nitroreducens* EF-2 and EF-2-H595N (abbreviated as *Mn*EF-2 and *Mn*EF-2-H595N, respectively) bound to GMPPCP and magnesium. The structures are shown to display compact conformations with a combination of domain interfaces seen thus far only in cryo-EM structures of SNU114, the eukaryotic spliceosomal GTPase (Nguyen et al., 2015; Wan et al., 2016; Yan et al., 2015). A structure of a second crystal form of *Mn*EF-2-H595N is reported that demonstrates large movements of domains IV and V relative to domains I-III and how crystal packing can stabilize more open conformations. The structures of *Mn*EF-2/*Mn*EF-2-H595N are shown to display P-loop, switch I, and switch II conformations, and an arrangement of domains I-III that are similar to those observed in ribosome-bound structures containing GMPPCP, suggesting an "on" state. Structural determinants of the "on" state are suggested through comparisons of structures with different degrees of ordering in switch I.

2. Materials and methods

2.1. Protein expression and purification

Crystals of *Mn*EF-2 and *Mn*EF-2-H595N bound to GMPPCP and magnesium were obtained during structural studies of the complex formation of EF-2 and diphthamide biosynthetic enzyme 2 (Dph2) that made extensive use of a Vinyl Anaerobic Chamber (Coy Laboratory Products, Inc.) for protein purification and crystallization (Fenwick et al., 2019). *Mn*EF-2 was prepared separately whereas *Mn*EF-2-H595N was coexpressed with *Mn*Dph2.

A gene encoding *Mn*EF-2 with a tobacco etch virus (TEV) protease-cleavable His_6-tag, codon-optimized for expression in *Escherichia coli*, was cloned into pET-28a(+) using NcoI and NotI restriction sites for overexpression of the product NH_2-MGSDKIHHHHHHSSGENLYFQGSGM$_1$ … P_{729}–COOH. Competent *E. coli* NiCo21(DE3) cells were transformed with plasmid pET-28a(+)-His_6-*Mn*EF-2 and spread onto agar plates containing Lysogeny Broth (LB) medium and kanamycin (40 mg/L). Large-scale cultures were grown in 3L shaker flasks containing 1.35 L of LB medium by rotation at 200 rpm and 37 °C. When the optical density at 600 nm (OD_{600}) reached 0.8–0.9, the flasks were moved to a cold room set at 4 °C for 2 h. Isopropyl β-D-1-thiogalactopyranoside (IPTG) was then added to the cultures to a final concentration of 0.5 mM, and the flasks were rotated at 200 rpm and 15 °C for 20 h. The cultures were moved to ice and centrifuged at 6000 g and 4 °C for 15 min, and the cell pellets were flash frozen in liquid nitrogen.

The cell pellets were thawed and resuspended in lysis buffer [20 mM Tris, 500 mM NaCl, 23 mM imidazole, 2.5 mM dithiothreitol (DTT), 0.3 mg/mL lysozyme, 28 units/mL benzonase (Sigma; ≥ 250 units/μL), pH 7.5] and then sonicated while kept on ice. The lysate was centrifuged at 50,000×*g* and 4 °C for 30 min and the supernatant was subjected to immobilized nickel chelate chromatography using wash (20 mM Tris, 500 mM NaCl, 23 mM imidazole, 2.5 mM DTT, pH 7.5) and elution (20 mM Tris, 500 mM NaCl, 340 mM imidazole, 0.8 mM DTT, pH 7.5) buffers. The protein eluate was subjected to size exclusion chromatography using a HiLoad 26/600 Superdex200 column (GE Healthcare Life Sciences) equilibrated with His_6-tag cleavage buffer (20 mM HEPES, 200 mM NaCl, 2 mM DTT, pH 7.5) and then incubated with TEV protease overnight at 18 °C. The reaction mixture was subjected to subtractive nickel chelate chromatography followed by size exclusion chromatography (using the buffers employed in the earlier chromatography steps) and then concentrated to 7 mL. The sample was moved into the anaerobic chamber, passed over Bio-Rad Econo Pac 10DG desalting columns equilibrated with 5 mM HEPES, 28 mM NaCl, pH 7.0, and flash frozen in liquid nitrogen. The final concentration of *Mn*EF-2 was estimated to be 0.21 mM based on the absorbance at 280 nm (A_{280}) and an extinction coefficient of 28,500 $M^{-1}cm^{-1}$.

Codon-optimized genes encoding *Mn*EF-2-H595N with a TEV protease-cleavable His_6-tag and *Mn*Dph2 were cloned into pETDuet-1 using NcoI-NotI and NdeI-XhoI restriction sites for overexpression of the products NH_2-MGSDKIHHHHHHSSGENLYFQGSGM$_1$ … N$_{595}$ … P$_{729}$–COOH and NH_2-M$_1$ … K$_{334}$–COOH, respectively. Competent *E. coli* NiCo21(DE3) cells were transformed with plasmid pSuf (Hanzelmann et al., 2004), made competent again and transformed with plasmid pETDuet-1-*Mn*EF-2-H595N-*Mn*Dph2, and spread onto agar plates containing LB medium, ampicillin (100 mg/L), and chloramphenicol (34 mg/L). Large-scale cultures were grown in 3L shaker flasks containing 1.8 L of selective minimal medium (1 × minimal medium salts, 100 mg/L ampicillin, 34 mg/L chloramphenicol, 6 g/L dextrose, 3 mM $MgSO_4$, and 0.1 mM $CaCl_2$) by rotation at 180 rpm and 37 °C. When the OD_{600} reached 0.5–0.55, the flasks were moved to a cold room set at 4 °C for 2.5 h. L-Cys, $Fe(NH_4)_2(SO_4)_2$, and IPTG were then added to the cultures to final concentrations of 0.29 mM, 0.089 mM, and 0.18 mM, respectively, and the cultures were rotated at 50 rpm and 15 °C for 20 h. The cultures were chilled in a 4 °C cold room, pelleted by centrifugation at 6000 g and 4 °C for 15 min, and flash frozen in liquid nitrogen.

The cell pellets were thawed in the anaerobic chamber, resuspended in lysis buffer (25 mM Tris, pH 7.4, 75 mM NaCl, 5 mM DTT, 0.4 mg/mL lysozyme, and 1.9 kU benzonase) and sonicated while kept on ice. The lysate was sealed in centrifuge bottles and removed from the anaerobic chamber for centrifugation at 60,000 g and 4 °C for 20 min. The spun lysate was placed back into the anaerobic chamber and the supernatant was subjected to immobilized nickel affinity chromatography using wash [25 mM Tris, pH 7.4, 75 mM NaCl, 2 mM DTT, and 0.2 mM *S*-adenosylhomocysteine (SAH)] and elution (25 mM Tris, pH 7.4, 75 mM NaCl, 15, 30, 90, 240, or 300 mM imidazole, 2 mM DTT, and 0.2 mM SAH) buffers. The protein eluate was buffer exchanged into protein storage buffer (5 mM HEPES and 40 mM NaCl, pH 7.0) using a Bio-Rad Econo-Pac 10DG desalting column and flash frozen in liquid nitrogen.

2.2. Crystallization

Protein crystals were grown using the hanging drop vapor diffusion method with drops formed by combining sample and reservoir solutions in a 1:1 ratio. The crystals were grown inside the anaerobic chamber, which was typically operated at room temperature (22 °C). For crystallization of *Mn*EF-2 and His_6-*Mn*EF-2-H595N bound to GMPPCP and magnesium, proteins samples were thawed and supplemented with GMPPCP (stored at 120 mM in 180 mM Tris base) and $MgCl_2$ at final concentrations of 9 and 15 mM, respectively. Crystals of *Mn*EF-2-GMPPCP-Mg^{2+} were obtained using reservoir solutions containing 100 mM HEPES or imidazole, pH 8.3, 200 mM sodium malonate, and 16–18% (w/v) polyethylene glycol (PEG) 4000. These crystals were cryoprotected by increasing the concentration of PEG4000 to 40% (w/v). Crystals of His_6-*Mn*EF-2-H595N-GMPPCP-Mg^{2+} were obtained using reservoir solutions containing 100 mM HEPES, pH 7.1–7.6, 200 mM ammonium sulfate, 5–15% (v/v) isopropanol, and 16.5–20% (w/v) PEG4000. The cryoprotectant solutions contained 100 mM HEPES, pH 7.1, 200 mM ammonium sulfate, 15 mM $MgCl_2$, 1.8 mM GMPPCP, 7.5 mM SAH (stored at 300 mM in dimethylsulfoxide), and either 39% (w/v) PEG4000 (*P*1 crystal form), or 22% (w/v) PEG4000, 8% (v/v) glycerol, and 9% (v/v) ethylene glycol ($P2_1$ crystal form).

2.3. Data collection and structure determination

X-ray diffraction experiments were performed at Northeastern Collaborative Access beamline 24-ID-C of the Advanced Photon Source (APS), which was equipped with a PILATUS 6M-F detector. The experiments used X-rays having a wavelength of 0.979 Å and an oscillation range of 0.2°. The crystal of *Mn*EF-2 and the two crystals of *Mn*EF-2-H595N corresponding to the reported structures were placed 500, 260, and 440 mm from the detector and X-ray data were collected over phi angular ranges of 280, 220, and 180°, respectively. Reflections were processed using HKL2000 (Otwinoski and Minor, 1997), XDS (Kabsch, 2010), AIMLESS (Evans and Murshudov, 2013), and SCALA (Evans, 2006).

Initial phases were obtained by molecular replacement using PHASER (McCoy et al., 2007) within PHENIX (Adams et al., 2011). The structure of *Sc*EF-2 (PDB entry 1N0V) (Jorgensen et al., 2003) was used as the search model for the structure of triclinic *Mn*EF-2-H595N. This structure was then used as the search model for determining the initial phases for the structures of *Mn*EF-2 and monoclinic *Mn*EF-2-H595N. Manual model building and automated structure refinement were carried out using COOT (Emsley et al., 2010) and PHENIX (Adams et al., 2011), respectively.

2.4. Figure preparation

Illustrations of crystal structures and electron density maps were prepared using CHIMERA (Pettersen et al., 2004) and PyMOL (DeLano, 2002).

3. Results

3.1. Crystal structure analysis

We determined a crystal structure of *Mn*EF-2 bound to GMPPCP and magnesium to 2.4 Å resolution and two crystal structures of His_6-tagged *Mn*EF-2-H595N bound to GMPPCP and magnesium to 1.4 and 2.1 Å resolution (Tables 1 and 2). The crystal of *Mn*EF-2 belonged to space group $P2_12_12_1$ and had an asymmetric unit containing two molecules of *Mn*EF-2 whereas the crystals of *Mn*EF-2-H595N belonged to space groups *P*1 and $P2_1$ and had asymmetric units containing one and two molecules of *Mn*EF-2-H595N, respectively. The associated electron density maps show strong electron density for all of the domains and ligands (Supplementary Material Fig. S1).

Switch I (residues 45–74) exhibits a variable degree of ordering whereas switch II (residues 92–111) is well ordered and structurally invariant. For the crystals of *Mn*EF-2-H595N, there is strong electron density for residues 45–49 and 57–74, with residues 63–68 showing a well-ordered α-helix. For the crystals of *Mn*EF-2, electron density is visible for all switch I residues in one molecule but only for residues 70–74 in the second molecule. Residues 63–67 and residues 49–57 of the more ordered switch I form an α-helix and two 3_{10} helices, respectively. However, the electron density is very weak for residues 59–69 and the α-helix is distorted and rotated relative to those in the crystals of *Mn*EF-2-H595N, which appears to be due to an interaction between residues 54–62 and a symmetry-related molecule of *Mn*EF-2. Our structure

Table 1
Data collection statistics.

	*Mn*EF-2 GMPPCP Mg^{2+}	*Mn*EF-2-H595N GMPPCP Mg^{2+} (*P*1)	*Mn*EF-2-H595N GMPPCP Mg^{2+} ($P2_1$)
PDB ID	6U45	6U43	6U44
Beamline	APS 24-ID-C	APS 24-ID-C	APS 24-ID-C
Wavelength (Å)	0.9791	0.9791	0.9791
Space group	$P2_12_12_1$	*P*1	$P2_1$
Unit cell dimensions (Å)	93.7, 134.4, 150.5	57.2, 62.5, 63.4	78.3, 106.8, 98.1
α, β, γ	90.0°, 90.0°, 90.0°	64.2°, 69.7°, 80.5°	90.0°, 105.5°, 90.0°
Resolution (Å)	150.5–2.35	56.3–1.40	94.5–2.10
Total number of reflections	816,917	292,475	294,383
Number of unique reflections	79,562	131,884	89,195
R_{merge} (%)	7.2 (71.5)[a]	4.4 (54.5)	8.6 (52.3)
$< I/\sigma(I) >$[b]	15.0 (1.2)[a]	9.7 (1.2)	7.7 (1.7)
Mean (I) half-set correlation CC(1/2)	0.998 (0.715)[a]	0.999 (0.720)	0.995 (0.791)
Completeness (%)	99.5 (93.1)[a]	90.3 (80.6)	98.4 (96.2)
Multiplicity	10.3 (4.9)[a]	2.2 (1.9)	3.3 (2.7)

[a] Values in parentheses refer to the highest resolution shell.
[b] Mean intensity of Bragg reflections divided by the standard deviation of intensity.

Table 2
Structure refinement statistics.

	*Mn*EF-2 GMPPCP Mg^{2+}	*Mn*EF-2-H595N GMPPCP Mg^{2+} (*P*1)	*Mn*EF-2-H595N GMPPCP Mg^{2+} ($P2_1$)
PDB ID	6U45	6U43	6U44
Number of reflections	79,362	131,860	89,111
Number of reflections in working set	75,369	125,346	84,729
R_{work}/R_{free} (%)	16.8/22.4	16.5/19.2	18.7/24.0
Number of protein atoms	10,968	5881	10,924
Number of ligand atoms	68	44	100
Number of water molecules	580	807	830
RMSD for bonds (Å)	0.008	0.015	0.007
RMSD for angles (°)	0.913	1.492	0.857
Ramachandran analysis			
Favored (%)	91.5	93.4	93.3
Allowed (%)	8.2	6.6	6.5
Generously allowed (%)	0.3	0.0	0.2

analysis thus focuses on the conformation of switch I of the high-resolution structure of *Mn*EF-2-H595N. For all five molecules of *Mn*EF-2/*Mn*EF-2-H595N, strong electron density is observed for switch II, which contains a portion of a β-strand (residues 92–94), a 3_{10} helix (residues 99–101), and an α-helix (residues 102–111).

3.2. Overall conformations

*Mn*EF-2 and *Mn*EF-2-H595N in the *P*1 crystal form display a similar compact conformation (Fig. 2A). Distinctively, domain III makes significant interactions with all of the other domains and there is no clear division into two superdomains despite the presence of flexible linkers connecting domain III to domains II and IV. Domains I and II and domains IV and V show their conserved interdomain arrangements (Aevarsson et al., 1994; Czworkowski et al., 1994; Jorgensen et al., 2003). Notably, domains II and IV pack together loosely (Supplementary Material Fig. S2) and the $P2_1$ crystal form of *Mn*EF-2-H595N shows less compact conformations stabilized via the packing of symmetry-related molecules between domains II-IV (Supplementary Material Fig. S3). Collectively, the *Mn*EF-2 and *Mn*EF-2-H595N conformations show a similar interdomain arrangement for domains I-III with a range of rotation in domains IV and V of 25° (Fig. 2B).

3.3. Interdomain interfaces

Domain III interacts with domain I by binding switch I and switch II. The interface involves salt bridges between Asp73 and Arg447, as well as Arg107 and Asp417, hydrogen bonding between the side chain of Asp100 and the backbone of His440, and a hydrophobic cluster formed by residues Ile70, Ile72, His98, Phe101, Leu439, and Ile443 (Fig. 2C). When switch I is ordered, the interface is augmented through interactions between the α-helix of switch I and the α-helix formed by residues 438–452 of domain III, including salt bridges between Arg68 and Glu442 and between Asp62 and Arg450 and Arg447 (Fig. 2D). In addition, Gly69 becomes ordered, making available its backbone carbonyl oxygen atom to coordinate a monovalent cation.

The interface between domains II and III is less extensive than that between domains I and III and contains mostly electrostatic interactions (Fig. 2E). These include a salt bridge formed between Glu306 and Lys415 and hydrogen bonds formed between Glu306 and Gln412 and Thr300 and Glu416.

The interface between domains III-V contains mostly nonpolar residues and most of the residues supplied by domain III reside on the linkers to domains II and IV (Fig. 2F). The linker connecting domains III and IV is short (relative to those in ribosome-bound structures of EF-2/EF-G, discussed below) due to backbone-backbone hydrogen bonding between Leu462 and Thr392 and Val464 and Val390, which extends the last β-strand of domain III beyond Pro461.

3.4. Active site structure

The active site of *Mn*EF-2/*Mn*EF-2-H595N is formed by residues that are part of five conserved GTP binding sequence motifs commonly found in G-proteins and known as G1 through G5 (Fig. 3A) (Sprang, 1997). The guanine moiety of GMPPCP is bound by residues of motifs G4 (F_{146}INKVD) and G5 (V_{199}AFGSAL). Hydrogen bonds are formed between N7 and the side chain of Asn148, between N1 and N2 and the side chain of Asp151, and between O6 and the side chain of Ser203 and the backbone amide nitrogen atom of Leu205. The triphosphate moiety is bound by Asp31, Gly33, Lys34, and Thr35 of the G1 motif/P-loop (residues 28–35; A_{28}HIDHGKT), Thr71 of the G2 motif (C-terminal loop of switch I; R_{68}GITIDS), and Thr36. The γ phosphate group is detected through hydrogen bonds with the backbone amide nitrogen atoms of Asp31 and Thr71 and through a salt bridge with the side chain of Lys34.

The essential magnesium ion coordinates with oxygen atoms of the β and γ phosphate groups, the side chain hydroxyl groups of Thr35 and Thr71, and two water molecules (Fig. 3A). No cation is observed at the monovalent cation site predicted by Kuhle and Ficner (2014). However, four atoms available to coordinate a cation – the oxygen atoms of the α and γ phosphate groups, the carbonyl oxygen atom of Gly69, and the side chain carboxylate group of Asp31 – form a nascent cation binding site (Fig. 3B). The water molecule believed to serve as an attacking nucleophile during hydrolysis donates hydrogen bonds to an oxygen atom of Pγ and to the carbonyl oxygen atom of Thr71 and accepts hydrogen bonds from the backbone amide nitrogen atoms of Gly97 and His98 from motif G3 (N-terminal half of switch II; L_{92}IDTPGHV) (Fig. 3C). In addition, the Nδ1 atom of the essential His98 forms a hydrogen bond with the backbone amide nitrogen atom of Asp100.

4. Discussion

4.1. Overall structure comparisons

The DALI server was used to align the compact conformations of *Mn*EF-2/*Mn*EF-2-H595N against structures in the PDB to identify similar

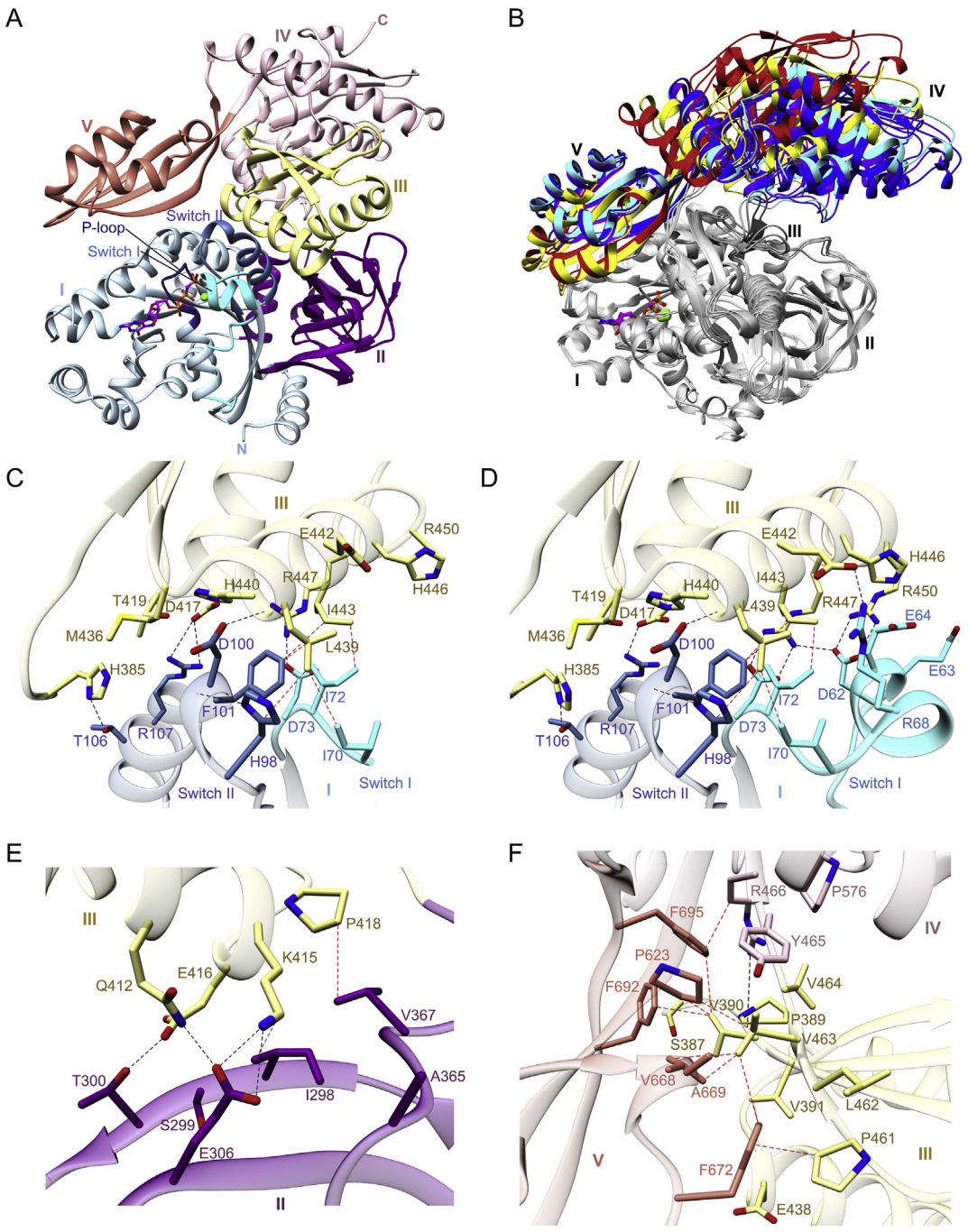

Fig. 2. Compact conformations of *Mn*EF-2 and *Mn*EF-2-H595N bound to GMPPCP and magnesium. (A) Ribbon representation of *Mn*EF-2-H595N (*P*1 crystal form). Domains are numbered using Roman numerals. The P-loop is colored dark slate blue, switch I cyan, and switch II steel blue. GMPPCP is shown as balls and sticks with carbon atoms colored magenta. Magnesium is shown as a green sphere. (B) Variability in overall conformation. Domains I-III of the five molecules of *Mn*EF-2/*Mn*EF-2-H595N (gray) are superimposed to highlight differences in movements of domains IV and V [*Mn*EF-2, blue and cyan; *Mn*EF-2-H595N (*P*1 crystal form), violet; *Mn*EF-2-H595N ($P2_1$ crystal form), yellow and red]. (C) Interface of domains I and III of molecule of *Mn*EF-2 having a mostly disordered switch I. (D) Interface of domains I and III of *Mn*EF-2-H595N (*P*1 crystal form) having an ordered switch I. (E) Interface of domains II and III of *Mn*EF-2-H595N (*P*1 crystal form). (F) Interface of domains III-V of *Mn*EF-2-H595N (*P*1 crystal form). Red dashed lines indicate hydrophobic contacts, and black dashed lines indicate possible electrostatic interactions (including salt bridges and hydrogen bonds).

conformations (Holm and Rosenstrom, 2010). Z scores above 30 were obtained for structures of spliceosomal GTPases *homo sapiens* SNU114 (EFTUD2), *Saccharomyces cerevisiae* SNU114, and *Schizosaccharomyces pombe* cwf10, in addition to ribosome-free structures of EF-2 and EF-G-2 (Supplementary Material Table S1). SNU114 is a known homologue of EF-2 containing five structural domains similar to EF-2 and an acidic N-terminal domain (Fabrizio et al., 1997). However, its overall structural similarity with EF-2 has not been previously demonstrated. Notably, the DALI computed optimal alignment lengths are higher and the RMSDs lower for the spliceosomal GTPases than for the EF-2 and EF-G structures. Accordingly, the compact conformations of *Mn*EF-2 superimpose well with SNU114 over all five domains (Fig. 4A and Supplementary Material Fig. S4) but only over domain subsets with structures of ribosome-bound and ribosome-free EF-2 and EF-G, which may be characterized as extended and partially extended, respectively (Fig. 4B and C).

The ribosome-bound structures of EF-2 and EF-G containing GMPPCP

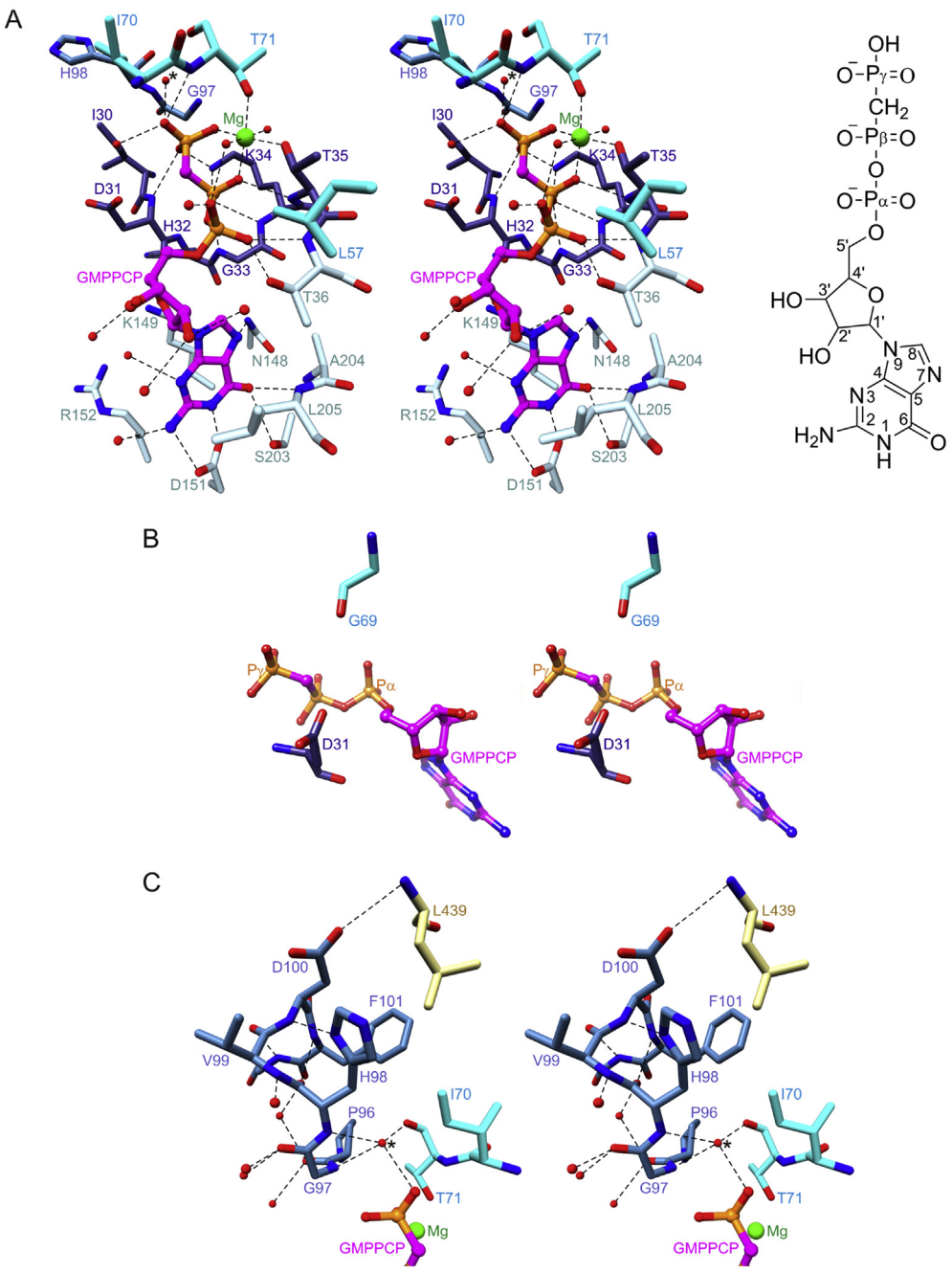

Fig. 3. Active site structure of *Mn*EF-2-H595N (*P*1 crystal form). (A) Stereo view of GMPPCP binding site. Magnesium (green sphere) displays an octahedral coordination sphere with separation distances of 2.1 Å from oxygen atoms of the side chains of Thr35 and Thr71, two water molecules, and the β phosphate of GMPPCP, and 2.0 Å from an oxygen atom of the γ phosphate of GMPPCP (left). Chemical structure and atom numbering of GMPPCP (right). (B) Stereo view of putative monovalent cation binding site. Four of five atoms predicted to coordinate a monovalent cation are present, including oxygen atoms of the α and γ phosphate groups, the carboxylate group of Asp31, and the backbone carbonyl oxygen atom of Gly69. The fifth atom – the oxygen atom bridging Pβ and Pγ – is replaced by a methylene group in GMPPCP. (C) Stereo view of portion of switch II near Pγ of GMPPCP. Water molecules are shown as red spheres. Dashed lines indicate possible electrostatic interactions, including hydrogen bonds. The asterisks in panels A and C denote the water serving as the attacking nucleophile.

(Pulk and Cate, 2013; Tourigny et al., 2013; Chen et al., 2013a; Pellegrino et al., 2018) have an interdomain arrangement of domains I-III like those of *Mn*EF-2/*Mn*EF-2-H595N and form a similar interface between domain III and switch I and II (Fig. 4B and D). However, domains IV and V are moved into the A-site of the ribosome, the hydrophobic interface between domains III-V observed in *Mn*EF-2/*Mn*EF-2-H595N is disrupted, and the linker between domains III and IV is longer due to loss of the β-strand extension at the end of domain III. In contrast, ribosome-free structures of EF-2 and EF-G maintain the hydrophobic interface between domains III-V, but lack the interface between domains I and III due to disorder in the switch regions (Fig. 4C and E) (Jorgensen et al., 2003; Hansson et al., 2005a; Laurberg et al., 2000; Tanzawa et al., 2018). Notably, ribosome-bound structures of EF-G containing GDP have conformations in which both the hydrophobic interface between domains III-V and the interface between domains I and III are disrupted (Gao et al., 2009; Zhou et al., 2013; Lin et al., 2015).

The structure of *Tt*EF-G-2-GTP-Mg^{2+} (PDB entry 1WDT) (Connell et al., 2007) is the only other available ribosome-free structure of a ribosomal translocase that has a GTP/GTP analog bound and switch I ordered. EF-G-2 is a homologue of EF-G which has been demonstrated to catalyze poly(U)-dependent poly-Phe synthesis (Connell et al., 2007) and lacks the essential active site histidine and the aspartate and glycine residues of the monovalent cation binding motif. The switch I and II structures and interdomain arrangement of domains I-III are similar to those of *Mn*EF-2/*Mn*EF-2-H595N. However, the hydrophobic interface between domains III-V is absent resulting in a partially extended conformation (Supplementary Material Fig. S5A) that is similar to ribosome-bound structures of EF-G stalled via binding a GTP analog (Connell et al., 2007). Notably, crystal packing shows a symmetry related copy of *Tt*EF-G-2 inserted between domains III and IV raising the possibility that the conformation is stabilized by crystal contacts.

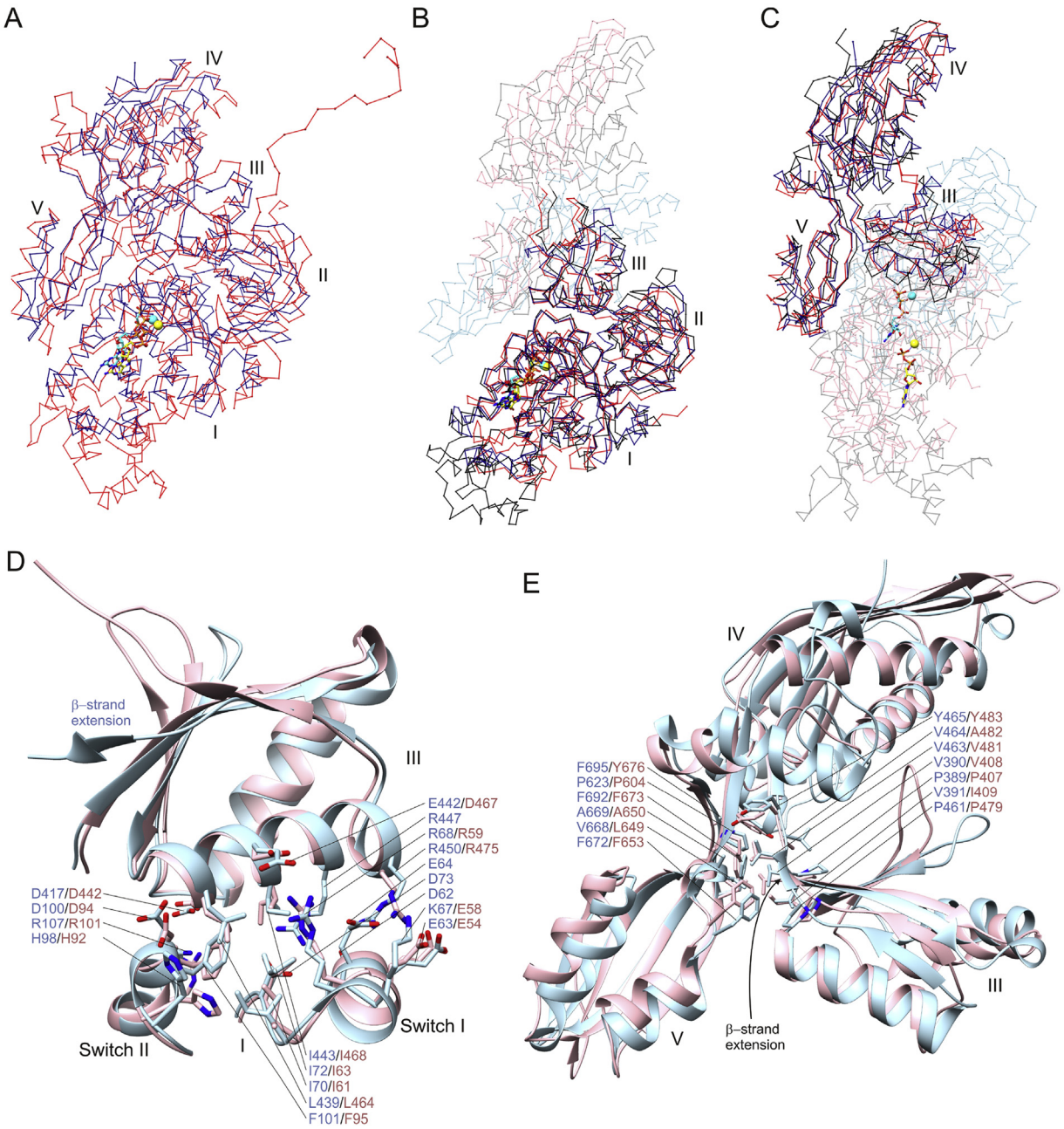

Fig. 4. Comparisons of interdomain arrangements and interfaces. (A) Similar interdomain arrangements of *Mn*EF-2-H595N-GMPPCP-Mg^{2+} ($P2_1$ crystal form; blue) and spliceosomal *Sc*SNU114 (PDB entry 5GMK; red) (Wan et al., 2016), shown as superimposed Cα atom traces. (B) Similar interdomain arrangements of domains I-III of *Mn*EF-2-H595N-GMPPCP-Mg^{2+} (*P*1 crystal form; blue) and ribosome-bound structures of *Sc*EF-2-GMPPCP (PDB entry 6GQV; black) (Pellegrino et al., 2018) and *Ec*EF-G-GMPPCP-Mg^{2+} (PDB entry 4V9O; red) (Pulk and Cate, 2013), shown as superimposed Cα atom traces. (C) Similar interdomain arrangements of domains III-V of *Mn*EF-2-H595N-GMPPCP-Mg^{2+} (*P*1 crystal form; blue) and ribosome-free structures of *Sc*EF-2 (PDB entry 1N0V; black) (Jorgensen et al., 2003) and *Tt*EF-G-H573A-GDP-Mg^{2+} (PDB entry 1FNM; red) (Laurberg et al., 2000), shown as superimposed Cα atom traces. (D) Similar interfaces between domains I-III of *Mn*EF-2-H595N-GMPPCP-Mg^{2+} (*P*1 crystal form; light blue ribbons and sticks) and ribosome-bound *Ec*EF-G-GMPPCP-Mg^{2+} (PDB entry 4V9O; pink ribbons and sticks) (Pulk and Cate, 2013). (E) Similar interfaces between domains III-V of *Mn*EF-2-H595N-GMPPCP-Mg^{2+} (*P*1 crystal form; light blue ribbons and sticks) and ribosome-free *Tt*EF-G-H573A-GDP-Mg^{2+} (PDB entry 1FNM; pink ribbons and sticks) (Laurberg et al., 2000).

Despite the available partially extended conformations of ribosome-free *Sc*EF-2 (Jorgensen et al., 2003), *Pyrococcus horikoshii* EF-2 (Tanzawa et al., 2018), and *Tt*EF-G (Aevarsson et al., 1994; Czworkowski et al., 1994; al-Karadaghi et al., 1996; Hansson et al., 2005a; Laurberg et al., 2000; Hansson et al., 2005b), crystal structures of ribosome-free *Staphylococcus aureus* EF-G (Koripella et al., 2012; Chen et al., 2010) favor the possibility of a compact conformation for EF-G having a similar domain arrangement as that observed in the structures of *Mn*EF-2/*Mn*EF-2-H595N. The structure of the fusidic acid hypersensitivity mutant *Sa*EF-G-M16I (PDB entry 3ZZ0) (Koripella et al., 2012) displays a similar overall domain arrangement and similar interfaces between domains III-V and between domains II and III, although it is less compact and contains a different switch II structure and a mostly disordered switch I (Supplementary Material Fig. S5B). The differences are likely to be due, at least in part, to the lack of a bound nucleotide.

Notably, a unique compact conformation of *Tt*EF-G-GDP-Mg^{2+} bound to the classical non-rotated state of the ribosome containing an A-site tRNA was recently reported by Lin et al. (PDB entry 4WPO) (Lin et al.,

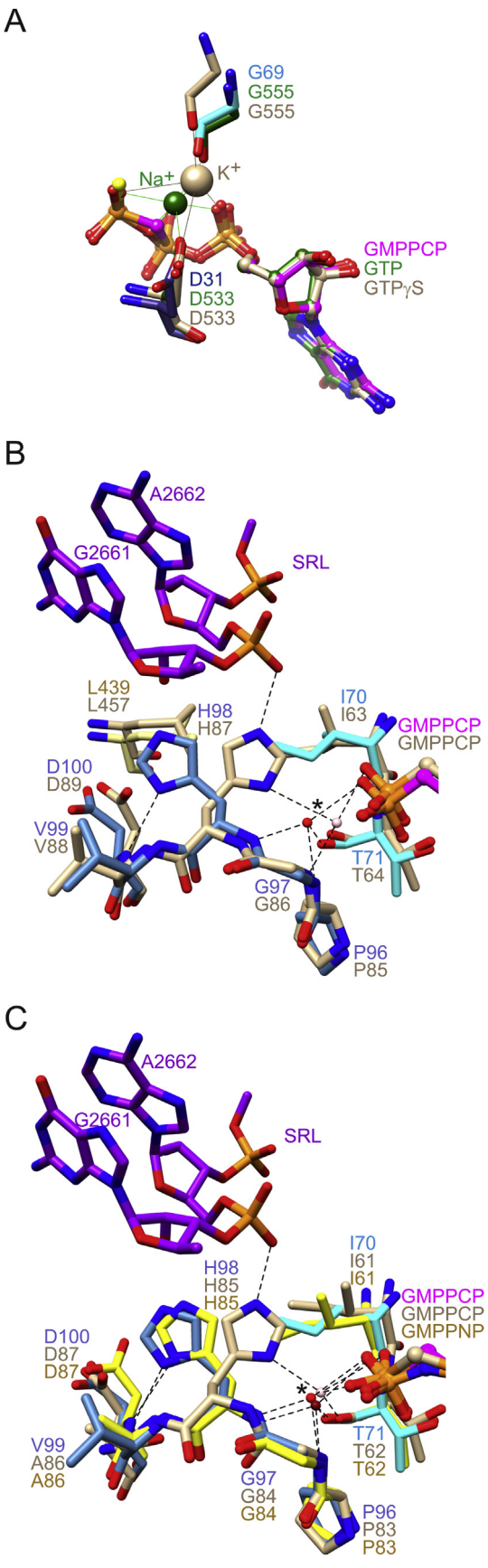

(caption on next column)

2015). The conformation has a similar interdomain arrangement of domains III-V as that of *Mn*EF-2/*Mn*EF-2-H595N. However, its switch I is disordered and the orientation of domains III-V relative to domains I-II differs by a rotation of about 150°, which positions domain III far from switch I and switch II (Fig. S5C). Differences between this compact conformation and those of *Mn*EF-2/*Mn*EF-2-H595N bound to GMPPCP are likely related to the fact that EF-G-GTP binds more favorably to the rotated ribosome from which translocation proceeds (Chen et al., 2013b).

4.2. Active site determinants of the interdomain arrangement of domains I-III

In ribosome-free structures of *Tt*EF-G bound to GDP and magnesium, the side chain of Lys25 in the P-loop points away from GDP and makes electrostatic interactions with switch II, including hydrogen bonds with the backbone and side chain of Thr84 and a salt bridge with Asp83 (Czworkowski et al., 1994; Laurberg et al., 2000). In contrast, in both ribosome-free structures of *Mn*EF-2/*Mn*EF-2-H595N and ribosome-bound structures of *Tt*EF-G bound to GMPPCP and magnesium, the P-loop lysine folds back to form salt bridges with Pβ and Pγ and is within hydrogen bonding distance of the backbone carbonyl oxygen atoms of Ala28/Ala19 and His29/His20 (Tourigny et al., 2013). In addition, Pγ forms a hydrogen bond with the backbone of Thr71/Thr64 of switch I and coordinates with magnesium, and Asp94/Asp83 of switch II makes second sphere interactions with a water molecule and Thr35/Thr26, which bind magnesium. These structural changes are associated with close positioning of switch II near Pγ for binding the water molecule serving as a nucleophile and with formation of a 3–10 helix by residues Val99, Asp100, and Phe101 in *Mn*EF-2/*Mn*EF-2-H595N. The side chain of Asp100 forms a hydrogen bond with the backbone amide nitrogen atom of His440 at the N-terminal end of the second α-helix of domain III which, together with salt bridges between Asp73 and Arg447 and between Arg107 and Asp417 and hydrophobic interactions between domains I and III, stabilize the interdomain arrangement of domains I and III (Fig. 2C). The arrangement is further stabilized through interactions introduced by the ordering of the switch I α-helix (Fig. 2D), which also orients the backbone carbonyl oxygen atom of Gly69 for binding a monovalent cation together with the side chain of Asp31 and the triphosphate group of the nucleotide. Four of the five predicted cation binding atoms in the structures of *Mn*EF-2-H595N occupy similar locations as the corresponding atoms in the structures of eIF5B-GTP-Mg^{2+}-Na^{+} and eIF5B-GTPγS-Mg^{2+}-K^{+} (PDB entries 4TMW and 4TMZ, respectively (Kuhle and Ficner, 2014); Fig. 5A). In accordance with previous predictions (Kuhle and Ficner, 2014), cation binding appears to be prevented by the presence of the methylene group between Pβ and Pγ of GMPPCP.

Despite the structural similarities in domains I-III of ribosome-free *Mn*EF-2/*Mn*-EF-2 and ribosome-bound *Tt*EF-G, a major difference

Fig. 5. Comparisons of active site structures of *Mn*EF-2-H595N, EF-G, EF-Tu, and eIF5B. (A) Similarity of putative monovalent cation binding site in *Mn*EF-2-H595N-GMPPCP-Mg^{2+} (*P*1 crystal form), the sodium ion (dark green sphere) binding site of eIF5B-GTP-Mg^{2+}-Na^{+} {PDB entry 4TMW (dark green) (Kuhle and Ficner, 2014)}, and the potassium ion (tan sphere) binding site of eIF5B-GTPγS-Mg^{2+}-K^{+} {PDB entry 4TMZ (tan) (Kuhle and Ficner, 2014)}. (B) Different side chain conformations of His98 in *Mn*EF-2-H595N-GMPPCP-Mg^{2+} (*Mn*EF-2 shows a similar conformation) and His87 in ribosome-bound *Tt*EF-G-GMPPCP-Mg^{2+} (PDB entry 4V9H (Tourigny et al., 2013); tan). A portion of the SRL of 23S rRNA is shown in purple. (C) Side chain conformation of His98 of *Mn*EF-2-H595N-GMPPCP-Mg^{2+} differs from that of His85 of ribosome-bound *Tt*EF-Tu-GMPPCP-Mg^{2+} (PDB entry 4V5L (Voorhees et al., 2010), tan), but is similar to that of His85 of ribosome-free *Tt*EF-Tu-GMPPNP-Mg^{2+} (PDB entry 1EFT (Kjeldgaard et al., 1993), yellow). The asterisks in panels B and C denote the water molecule serving as the attacking nucleophile, which is shown as a pink, red, or dark red sphere. Dashed lines indicate potential hydrogen bonds.

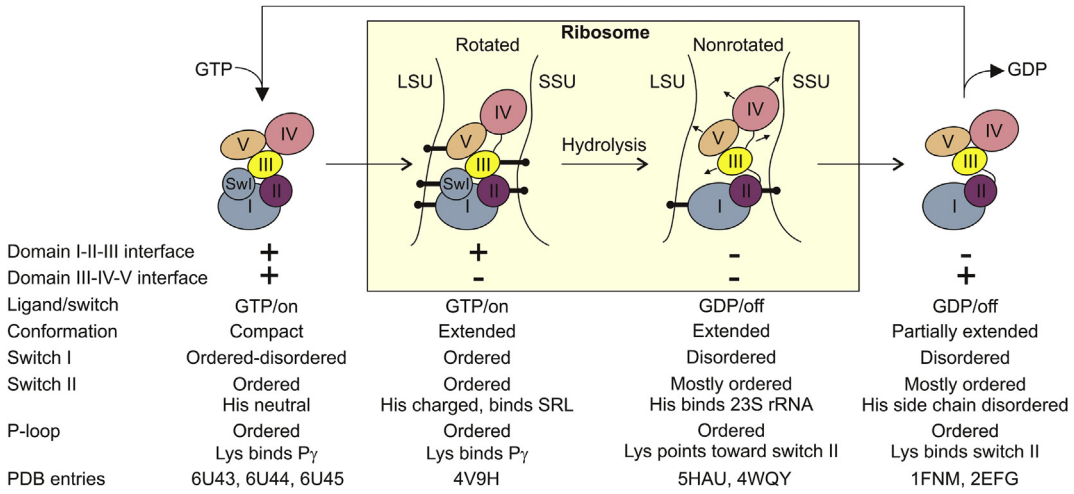

Fig. 6. Schematic representation of EF-2/EF-G conformations during translocation cycle showing a stepwise loss or gain of interfaces involving domain III. SwI, switch I.

occurs in the side chain conformation of His98/His87. In the ribosome-free structures, Nδ1 is within hydrogen bonding distance of the backbone of Asp100 (Fig. 5B) and the side chain is expected to be neutral. In contrast, in the ribosome-bound structures (Pulk and Cate, 2013; Tourigny et al., 2013; Voorhees et al., 2010), the side chain is oriented towards Pγ of the GTP analog with its Nε2 atom forming a hydrogen bond with the phosphate group of adenosine 2662 (*Tt*EF-G numbering) of the sarcin-ricin loop (SRL) of 23S rRNA and Nδ1 forming a hydrogen bond with the water molecule positioned for nucleophilic attack of Pγ (Fig. 5B). The histidine was initially proposed to act as a general base for accepting a proton from the water molecule (Voorhees et al., 2010) but was later argued to be positively charged and that Pγ instead acts as the general base (Adamczyk and Warshel, 2011; Liljas et al., 2011). Notably, a similar conformational change is observed between ribosome-free and ribosome-bound EF-Tu with the water molecule positioned for nucleophilic attack of Pγ predicted to be involved in similar hydrogen bonding interactions (Fig. 5C) (Kjeldgaard et al., 1993; Nissen et al., 1995). The results suggest that, similar to EF-Tu, EF-2 reduces the rate of GTP hydrolysis in the ribosome-free state by positioning the side chain of the switch II histidine away from Pγ, and increases the rate of GTP hydrolysis through protonation of the side chain and a conformational change induced in the ribosome-bound state that leads to hydrogen bond formation with the water molecule positioned for nucleophilic attack of Pγ.

5. Conclusions

The crystal structures presented in this study provide a first view of ribosome-free EF-2 bound to a GTP analog and magnesium. The structures expand the known conformational space of EF-2 and, together with other crystal structures of ribosome-free EF-2 and EF-G, suggest that these translocases undergo significant conformational changes in solution, with GTP and magnesium binding favoring compact states. Interactions between the γ phosphate of GMPPCP and the P-loop and switch I lead to structural changes that favor an interdomain arrangement of domains I-III similar to that bound to the ribosome. The interdomain arrangement promotes further ordering of the switch I α-helix in the ribosome-free state, consistent with a proteolysis study by Ticu et al. (2009), and formation of the monovalent cation binding site predicted by Kuhle and Ficner (2014) to play a catalytic role in GTP hydrolysis. However, the side chain of His98 in switch II is placed in a conformation and protonation state that is unfavorable for GTP hydrolysis, as observed with EF-Tu (Kjeldgaard et al., 1993; Nissen et al., 1995), suggesting that interactions with the SRL of the ribosome lead to the proper positioning of the side chain for catalyzing hydrolysis. In the compact ribosome-free state, domains IV and V display varying degrees of displacement relative to domains I-III (Fig. 2B) consistent with their ability to extend farther with the domain I-III interdomain arrangement maintained, as observed in ribosome-free *Tt*EF-G-2-GTP-Mg^{2+} (Connell et al., 2007) and in ribosome-bound structures of EF-2 and EF-G bound to GMPPCP (Pulk and Cate, 2013; Tourigny et al., 2013; Chen et al., 2013a; Pellegrino et al., 2018).

The compact conformations and active site architectures of *Mn*EF-2/*Mn*EF-2-H595N are consistent with a ribosome-free"on" state within the GTPase on/off switch paradigm (Vetter and Wittinghofer, 2001) and, together with other structures of ribosome-free and ribosome-bound EF-2 and EF-G, suggest a translocation cycle involving a stepwise loss and gain of interfaces with domain III (Fig. 6). Binding GTP and magnesium prearranges domains I-III for binding the rotated ribosome. Movement of domains IV and V towards the aminoacyl site is associated with the loss of the hydrophobic interface between domains III-V (Connell et al., 2007). GTP hydrolysis promotes the disordering of switch I and reduction of the interface between domains I and III (Gao et al., 2009), leading to domain III-V disordering (Lin et al., 2015; Mace et al., 2018), reverse rotation of the ribosome, and dissociation of the translocase (Chen et al., 2013b). The cycle is completed via formation of the hydrophobic interface between domains III-V, which is observed in structures of apo and GDP/GTP analog-bound EF-G and apo EF-2 (Aevarsson et al., 1994; Czworkowski et al., 1994; Jorgensen et al., 2003; Lin et al., 2015; Hansson et al., 2005a).

Conflict of interest

There is no conflict of interest.

Acknowledgments

The work is based upon research conducted at the Advanced Photon Source on the Northeastern Collaborative Access Team beamlines, which are supported by award P30 GM124165 from the NIH. Use of the Advanced Photon Source is supported by the U.S. Department of Energy, Office of Basic Energy Sciences, under Contract No. DE-AC02-06CH11357.

Appendix A. Supplementary data

Supplementary data to this article can be found online at https://doi.org/10.1016/j.crstbi.2020.02.001.

References

Adamczyk, A.J., Warshel, A., 2011. Converting structural information into an allosteric-energy-based picture for elongation factor Tu activation by the ribosome. Proc. Natl. Acad. Sci. U. S. A. 108, 9827–9832.

Adams, P.D., Afonine, P.V., Bunkoczi, G., Chen, V.B., Echols, N., Headd, J.J., Hung, L.W., Jain, S., Kapral, G.J., Grosse Kunstleve, R.W., et al., 2011. The Phenix software for automated determination of macromolecular structures. Methods 55, 94–106.

Aevarsson, A., Brazhnikov, E., Garber, M., Zheltonosova, J., Chirgadze, Y., al-Karadaghi, S., Svensson, L.A., Liljas, A., 1994. Three-dimensional structure of the ribosomal translocase: elongation factor G from Thermus thermophilus. EMBO J. 13, 3669–3677.

al-Karadaghi, S., Aevarsson, A., Garber, M., Zheltonosova, J., Liljas, A., 1996. The structure of elongation factor G in complex with GDP: conformational flexibility and nucleotide exchange. Structure 4, 555–565.

Ash, M.R., Maher, M.J., Guss, J.M., Jormakka, M., 2011. The initiation of GTP hydrolysis by the G-domain of FeoB: insights from a transition-state complex structure. PloS One 6, e23355.

Chappie, J.S., Mears, J.A., Fang, S., Leonard, M., Schmid, S.L., Milligan, R.A., Hinshaw, J.E., Dyda, F., 2011. A pseudoatomic model of the dynamin polymer identifies a hydrolysis-dependent powerstroke. Cell 147, 209–222.

Chen, Y., Koripella, R.K., Sanyal, S., Selmer, M., 2010. Staphylococcus aureus elongation factor G–structure and analysis of a target for fusidic acid. FEBS J. 277, 3789–3803.

Chen, Y., Feng, S., Kumar, V., Ero, R., Gao, Y.G., 2013a. Structure of EF-G-ribosome complex in a pretranslocation state. Nat. Struct. Mol. Biol. 20, 1077–1084.

Chen, J., Petrov, A., Tsai, A., O'Leary, S.E., Puglisi, J.D., 2013b. Coordinated conformational and compositional dynamics drive ribosome translocation. Nat. Struct. Mol. Biol. 20, 718–727.

Connell, S.R., Takemoto, C., Wilson, D.N., Wang, H., Murayama, K., Terada, T., Shirouzu, M., Rost, M., Schuler, M., Giesebrecht, J., et al., 2007. Structural basis for interaction of the ribosome with the switch regions of GTP-bound elongation factors. Mol. Cell 25, 751–764.

Czworkowski, J., Wang, J., Steitz, T.A., Moore, P.B., 1994. The crystal structure of elongation factor G complexed with GDP, at 2.7 A resolution. EMBO J. 13, 3661–3668.

DeLano, W.L., 2002. The PyMOL Molecular Graphics System. DeLano Scientific, San Carlos, CA.

Emsley, P., Lohkamp, B., Scott, W.G., Cowtan, K., 2010. Features and development of Coot. Acta Crystallogr. D66, 486–501.

Evans, P., 2006. Scaling and assessment of data quality. Acta Crystallogr. D62, 72–82.

Evans, P.R., Murshudov, G.N., 2013. How good are my data and what is the resolution? Acta Crystallogr. D69, 1204–1214.

Fabrizio, P., Laggerbauer, B., Lauber, J., Lane, W.S., Luhrmann, R., 1997. An evolutionarily conserved U5 snRNP-specific protein is a GTP-binding factor closely related to the ribosomal translocase EF-2. EMBO J. 16, 4092–4106.

Fenwick, M.K., Dong, M., Lin, H., Ealick, S.E., 2019. The crystal structure of Dph2 in complex with elongation factor 2 reveals the structural basis for the first step of diphthamide biosynthesis. Biochemistry 58, 4343–4351.

Frank, J., Agrawal, R.K., 2000. A ratchet-like inter-subunit reorganization of the ribosome during translocation. Nature 406, 318–322.

Gao, Y.G., Selmer, M., Dunham, C.M., Weixlbaumer, A., Kelley, A.C., Ramakrishnan, V., 2009. The structure of the ribosome with elongation factor G trapped in the posttranslocational state. Science 326, 694–699.

Hansson, S., Singh, R., Gudkov, A.T., Liljas, A., Logan, D.T., 2005a. Crystal structure of a mutant elongation factor G trapped with a GTP analogue. FEBS Lett. 579, 4492–4497.

Hansson, S., Singh, R., Gudkov, A.T., Liljas, A., Logan, D.T., 2005b. Structural insights into fusidic acid resistance and sensitivity in EF-G. J. Mol. Biol. 348, 939–949.

Hanzelmann, P., Hernandez, H.L., Menzel, C., Garcia-Serres, R., Huynh, B.H., Johnson, M.K., Mendel, R.R., Schindelin, H., 2004. Characterization of MOCS1A, an oxygen-sensitive iron-sulfur protein involved in human molybdenum cofactor biosynthesis. J. Biol. Chem. 279, 34721–34732.

Hauryliuk, V., Hansson, S., Ehrenberg, M., 2008. Cofactor dependent conformational switching of GTPases. Biophys. J. 95, 1704–1715.

Holm, L., Rosenstrom, P., 2010. Dali server: conservation mapping in 3D. Nucleic Acids Res. 38, W545–W549.

Jorgensen, R., Ortiz, P.A., Carr-Schmid, A., Nissen, P., Kinzy, T.G., Andersen, G.R., 2003. Two crystal structures demonstrate large conformational changes in the eukaryotic ribosomal translocase. Nat. Struct. Biol. 10, 379–385.

Kabsch, W., 2010. XDS. Acta Crystallogr. D66, 125–132.

Kaziro, Y., 1978. The role of guanosine 5'-triphosphate in polypeptide chain elongation. Biochim. Biophys. Acta 505, 95–127.

Kjeldgaard, M., Nissen, P., Thirup, S., Nyborg, J., 1993. The crystal structure of elongation factor EF-Tu from Thermus aquaticus in the GTP conformation. Structure 1, 35–50.

Koripella, R.K., Chen, Y., Peisker, K., Koh, C.S., Selmer, M., Sanyal, S., 2012. Mechanism of elongation factor-G-mediated fusidic acid resistance and fitness compensation in Staphylococcus aureus. J. Biol. Chem. 287, 30257–30267.

Korostelev, A., Ermolenko, D.N., Noller, H.F., 2008. Structural dynamics of the ribosome. Curr. Opin. Chem. Biol. 12, 674–683.

Kuhle, B., Ficner, R., 2014. A monovalent cation acts as structural and catalytic cofactor in translational GTPases. EMBO J. 33, 2547–2563.

Laurberg, M., Kristensen, O., Martemyanov, K., Gudkov, A.T., Nagaev, I., Hughes, D., Liljas, A., 2000. Structure of a mutant EF-G reveals domain III and possibly the fusidic acid binding site. J. Mol. Biol. 303, 593–603.

Liljas, A., Ehrenberg, M., Aqvist, J., 2011. Comment on "The mechanism for activation of GTP hydrolysis on the ribosome". Science 333, 37 author reply 37.

Lin, J., Gagnon, M.G., Bulkley, D., Steitz, T.A., 2015. Conformational changes of elongation factor G on the ribosome during tRNA translocation. Cell 160, 219–227.

Mace, K., Giudice, E., Chat, S., Gillet, R., 2018. The structure of an elongation factor G-ribosome complex captured in the absence of inhibitors. Nucleic Acids Res. 46, 3211–3217.

Martemyanov, K.A., Liljas, A., Yarunin, A.S., Gudkov, A.T., 2001. Mutations in the G-domain of elongation factor G from Thermus thermophilus affect both its interaction with GTP and fusidic acid. J. Biol. Chem. 276, 28774–28778.

McCoy, A.J., Grosse-Kunstleve, R.W., Adams, P.D., Winn, M.D., Storoni, L.C., Read, R.J., 2007. Phaser crystallographic software. J. Appl. Crystallogr. 40, 658–674.

Nguyen, T.H., Galej, W.P., Bai, X.C., Savva, C.G., Newman, A.J., Scheres, S.H., Nagai, K., 2015. The architecture of the spliceosomal U4/U6.U5 tri-snRNP. Nature 523, 47–52.

Nissen, P., Kjeldgaard, M., Thirup, S., Polekhina, G., Reshetnikova, L., Clark, B.F., Nyborg, J., 1995. Crystal structure of the ternary complex of Phe-tRNAPhe, EF-Tu, and a GTP analog. Science 270, 1464–1472.

Otwinoski, Z., Minor, W., 1997. Processing of X-ray diffraction data collected in oscillation mode. Methods Enzymol. 276, 307–326.

Pellegrino, S., Demeshkina, N., Mancera-Martinez, E., Melnikov, S., Simonetti, A., Myasnikov, A., Yusupov, M., Yusupova, G., Hashem, Y., 2018. Structural insights into the role of diphthamide on elongation factor 2 in mRNA reading-frame maintenance. J. Mol. Biol. 430, 2677–2687.

Pettersen, E.F., Goddard, T.D., Huang, C.C., Couch, G.S., Greenblatt, D.M., Meng, E.C., Ferrin, T.E., 2004. UCSF Chimera–a visualization system for exploratory research and analysis. J. Comput. Chem. 25, 1605–1612.

Pulk, A., Cate, J.H., 2013. Control of ribosomal subunit rotation by elongation factor G. Science 340, 1235970.

Sprang, S.R., 1997. G protein mechanisms: insights from structural analysis. Annu. Rev. Biochem. 66, 639–678.

Tanzawa, T., Kato, K., Girodat, D., Ose, T., Kumakura, Y., Wieden, H.J., Uchiumi, T., Tanaka, I., Yao, M., 2018. The C-terminal helix of ribosomal P stalk recognizes a hydrophobic groove of elongation factor 2 in a novel fashion. Nucleic Acids Res. 46, 3232–3244.

Ticu, C., Nechifor, R., Nguyen, B., Desrosiers, M., Wilson, K.S., 2009. Conformational changes in switch I of EF-G drive its directional cycling on and off the ribosome. EMBO J. 28, 2053–2065.

Tourigny, D.S., Fernandez, I.S., Kelley, A.C., Ramakrishnan, V., 2013. Elongation factor G bound to the ribosome in an intermediate state of translocation. Science 340, 1235490.

Vetter, I.R., Wittinghofer, A., 2001. The guanine nucleotide-binding switch in three dimensions. Science 294, 1299–1304.

Voorhees, R.M., Schmeing, T.M., Kelley, A.C., Ramakrishnan, V., 2010. The mechanism for activation of GTP hydrolysis on the ribosome. Science 330, 835–838.

Wan, R., Yan, C., Bai, R., Huang, G., Shi, Y., 2016. Structure of a yeast catalytic step I spliceosome at 3.4 A resolution. Science 353, 895–904.

Wintermeyer, W., Savelsbergh, A., Semenkov, Y.P., Katunin, V.I., Rodnina, M.V., 2001. Mechanism of elongation factor G function in tRNA translocation on the ribosome. Cold Spring Harbor Symp. Quant. Biol. 66, 449–458.

Yan, C., Hang, J., Wan, R., Huang, M., Wong, C.C., Shi, Y., 2015. Structure of a yeast spliceosome at 3.6-angstrom resolution. Science 349, 1182–1191.

Zhou, J., Lancaster, L., Donohue, J.P., Noller, H.F., 2013. Crystal structures of EF-G-ribosome complexes trapped in intermediate states of translocation. Science 340, 1236086.